Unmanned aerial vehicle (UAV) derived structure-from-motion photogrammetry point clouds for oil palm (*Elaeis guineensis*) canopy segmentation and height estimation

Dominic Fawcett[a,*], Azlan Benjamin[b], Timothy C. Hill[c], Lip Khoon Kho[d], Jon Bennie[a], Karen Anderson[a]

[a] Environment and Sustainability Institute, University of Exeter, Penryn, Cornwall TR10 9EZ, UK

[b] Geo-Information Department, Sarawak Oil Palms Berhad, 98007 Miri, Sarawak, Malaysia

[c] Department of Geography, University of Exeter, Rennes Drive, Exeter EX4 4RJ, UK

[d] Tropical Peat Research Institute, Biological Research Division, Malaysian Palm Oil Board, 43000 Selangor, Malaysia

* d.fawcett@exeter.ac.uk

Unmanned aerial vehicle (UAV) derived structure-from-motion photogrammetry point clouds for oil palm (*Elaeis guineensis*) canopy segmentation and height estimation

Abstract

The vast size of oil palm (*Elaeis guineensis*) plantations has led to lightweight unmanned aerial vehicles (UAVs) being identified as cost effective tools to generate inventories for improved plantation management, with proximal aerial data capable of resolving single palm canopies at potentially, centimetric resolution. If acquired with sufficient overlap, aerial data from UAVs can be processed within structure-from-motion (SfM) photogrammetry workflows to yield volumetric point cloud representations of the scene. Point cloud-derived structural information on individual palms can benefit not only plantation management but is also of great environmental research interest, given the potential to deliver spatially contiguous quantifications of aboveground biomass, from which carbon can be accounted. Using lightweight UAVs we captured data over plantation plots of varying ages (2, 7 and 10 years) at peat soil sites in Sarawak, Malaysia, and we explored the impact of changing spatial resolution and image overlap on spatially variable uncertainties in SfM derived point clouds for the ten year old plot. Point cloud precisions were found to be in the decimetre range (mean of 26.7 cm) for a 10 year old plantation plot surveyed at 100 m flight altitude and >75% image overlap. Derived canopy height models were used and evaluated for automated palm identification using local height maxima. Metrics such as maximum canopy height and stem height, derived from segmented single palm point clouds were tested relative to ground validation data. Local maximum identification performed best for palms which were taller than surrounding undergrowth but whose fronds did not overlap significantly (98.2% mapping accuracy for 7 year old plot of 776 palms). Stem heights could be predicted from point cloud derived metrics with root-mean-square errors (RMSEs) of 0.27 m (R^2= 0.63) for 7 year old and 0.45 m (R^2=0.69) for 10 year old palms. It was also found that an acquisition designed to yield the minimal required overlap between images (60%) performed almost as well as higher overlap acquisitions (>75%) for palm identification and basic height metrics which is promising for operational implementations seeking to maximise spatial coverage and minimise processing costs. We conclude that UAV-based SfM can provide reliable data not only for oil palm inventory generation but allows the retrieval of basic structural parameters which may enable per-palm above-ground biomass estimations.

1 Introduction

The oil palm (*Elaeis guineensis* Jacq.) can yield considerably more oil per hectare than any other crop, which explains its large-scale expansion over the last century, to meet the global demand for food and biofuel (Corley and Tinker 2016). As a result the conversion of forest ecosystems to oil palm plantations has been the topic of much international research and also controversy due to concerns regarding its impact on biodiversity, carbon storage and ecosystem services (Fitzherbert et al. 2008; Butler and Laurance 2009; Carlson et al. 2012; Germer and Sauerborn 2008; Koh and Wilcove 2008).

The global demand for oil palm products means that plantations now cover large tracts of land in the tropics – for example, in Malaysia 58,100 km^2 is taken up by commercial oil palm plantations (as of 1 December 2017, Malaysian Palm Oil Board (MPOB) statistics retrieved from http://bepi.mpob.gov.my).

Both at national and plantation block scale, remote sensing is a valuable tool both for stakeholders and researchers. To provide an example, remote sensing data offers a means by which plantation management can be performed in a more profitable and arguably more sustainable manner because plantation inventories can be generated to inform targeted fertiliser and pesticide application (Chong et al. 2017). Beyond the commercial sector, remote sensing data have been applied on a state-wide scale to monitor and quantify the impact of the land-use change due to the establishment of new plantations. These analyses are predominantly based on satellite data, and various studies have utilised optical, and radio detection and ranging (RADAR) capabilities to differentiate oil palm from other land cover classes (Morel et al. 2011; L. Li et al. 2015; Koh et al. 2011; Cheng et al. 2018). The challenge with using readily available satellite data for oil palm science is the limited spatial and/or temporal resolution of such data. The demand for finer spatial resolution data is motivated by the ability to resolve individual palm canopies, which can be used as reference data to improve land-cover classifications (Nomura and Mitchard 2018) and allows for automated identification and parameter retrieval to provide information about palm structure and status. These parameters are not only of interest for plantation management but are central to the estimation of plantation carbon stocks, e.g. through the use of allometric equations (Corley and Tinker 2016). Such work is critical from a scientific perspective if the carbon implications of forest conversion to oil palm are to be quantified accurately (Morel et al. 2011), and yet, there are missing examples of such methods in the literature. Furthermore, patterns relating to local soil nutrient deficiency or disease could also be better identified (Shafri and Hamdan 2009).

For inventory generation, fine spatial resolution satellite data (e.g. WorldView 4 at 0.31 m spatial resolution) provides fine resolution information, while enabling monitoring over a broad spatial extent and has been successfully used for palm identification (Weijia Li et al. 2016; Srestasathiern and Rakwatin 2014), but is not suitable for estimating structural parameters. For practical considerations, fine spatial resolution satellite data have known limitations, for example – they are financially costly and for countries with frequent cloud cover, acquiring a cloud-free acquisition at the desired time can be challenging. Improved accessibility, low operating costs, and ease of use has recently led to lightweight drone platforms (often called unmanned aerial vehicles or systems (UAV/UAS)) being identified as a useful tool in oil palm plantation management, with major commercial oil palm companies establishing dedicated UAV-teams for the routine acquisition of aerial imagery (pers. comm. Sarawak Oil Palms Berhad, 2018).

Currently the primary application of UAV data in oil palm management is the generation of photographic-based orthomosaics for inventory purposes (Rokhmana 2015). Manual identification based on spatial data products is still considered the most accurate and cost-effective method to generate inventories in commercial applications and the selection of training data in recent scientific applications (e.g. Nomura and Mitchard 2018). There are however promising first demonstrations of machine learning techniques on both fine spatial resolution satellite and UAV image data of oil palms and date palms respectively (Weijia Li et al. 2016; Malek et al. 2014) as well as software packages for the operational implementation of object-based segmentation (eCognition, Trimble, California, USA) for palm identification.

In these workflows, the third spatial dimension (i.e. height) has to date been completely disregarded for oil palm, however, its inclusion opens up many scientific and operational management possibilities at low opportunity cost. The acquisition of overlapping images from UAV platforms allows the application of a photogrammetric method which automatically solves for the geometry of the scene, camera positions and orientations, known as structure-from-motion (SfM) photogrammetry (Westoby et al. 2012). SfM can be used to generate fine spatial resolution orthomosaics, and point clouds representing the height structure of the scene (Dandois and Ellis 2013). Coupled with precise

georeferencing information, resultant point clouds can be used to spatially separate objects and determine their spatial and volumetric dimensions, in much the same way that light detection and ranging (LiDAR) data permit, but at lower acquisition costs. Such methods are now being used extensively to derive canopy metrics of individual vegetation canopies of varying sizes and structure (Puliti et al. 2015; Cunliffe, Brazier, and Anderson 2016; Zarco-Tejada et al. 2014), so it is a natural step to consider the utility of such approaches for oil palm inventory. Doing so would deliver new understanding of the volumetric characteristics of oil palm plantations, which would prove particularly useful for spatial carbon evaluations. Currently such aspects of oil palm plantations lack sufficient data from which to quantify the environmental effects of tropical forest conversion (Kho and Jepsen 2015). Information on palm height and its distribution is desirable as it can be an indicator of palm age and localised growing conditions. Variations due to re-planting of missing palms are expected to be small as this does generally not occur past the first year (Corley and Tinker 2016). More spatially contiguous variations can be the result of unequal fertiliser application or other variations, e.g. in soil nutrient availability. In previous work, UAV based photogrammetry derived top-of-canopy height metrics in other ecosystems were found to be comparable with LiDAR derived heights (Wallace et al. 2016; Thiel and Schmullius 2017), with data acquisition being comparably, more affordable (relying only on consumer grade sensors and platforms) and easy to deploy (so long as the aircraft and payload are lighter than the low weight categories defined by civil aviation classifications (Duffy et al. 2017)). First efforts in applying the UAV-based SfM methodology to palm plantations have demonstrated the potential for palm identification and retrieval of structural parameters (Kattenborn et al. 2014), however further investigation into uncertainties within generated products as well as the influence of acquisition schemes which allow to cover greater area at the cost of data quality is required for the operational implementation of these workflows.

Presented in this study is the first investigation of UAV and SfM-derived point clouds for oil palm plantation physical assessment. This application of UAV data extends beyond identification and counting of individual palms and presents a novel workflow for the segmentation of individual palm objects from point clouds to explore their application for retrieving height-related structural parameters, as well as quantify spatially-variable uncertainties. Specific aims of this study are:

a) To demonstrate a workflow for the retrieval of single palm canopies from SfM point clouds.
b) To quantify the uncertainties introduced by the acquisition scheme and steps in the SfM-based workflow as well as in the retrieved metrics.
c) To derive and assess top-frond-height (TFH) and stem height metrics from single palm SfM point clouds.

Aim b) is key to understanding the potential and limitations of our methodology for oil palm science. This is especially important when considering the possible further usage of the retrieved structural parameters (aim c)) to inform larger scale models, as has been successfully demonstrated for forestry (Puliti et al. 2017), to quantify error propagation. Aim c) provides an important step towards deriving per-palm above-ground biomass (AGB) (Corley and Tinker 2016; Thenkabail et al. 2004).

2 Materials and Methods

2.1 Study site

The study sites were located in the state of Sarawak, Malaysian Borneo, on the Sarawak Oil Palms Berhad plantations of Sabaju (3°09'40.1"N 113°25'09.1"E) and Sebungan (3°09'58.1"N 113°21'20.2"E). The majority of the plantation area was planted on tropical peat with smaller areas on clay dominated mineral soil. Three peat soil plantation sub-plots of 2, 7 and 10 years of age and covering approx. 4, 6 and 6 ha respectively were selected for this study. Plot sizes were chosen based on the maximal area which could be safely covered with one flight battery whilst also fulfilling the desired image acquisition

parameters (see section 2.2.2). The locations of the survey plots are depicted in

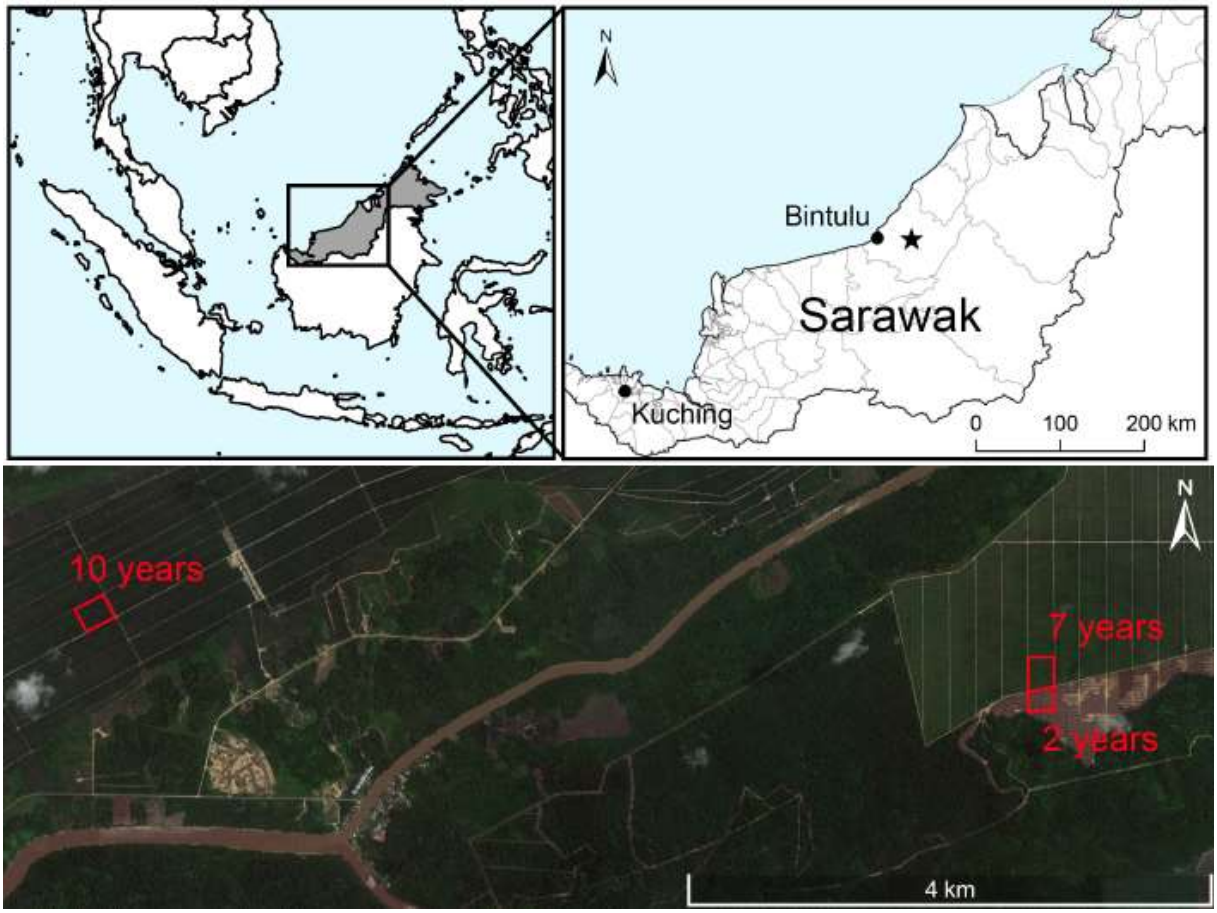

Figure *1*. These locations were selected to contain two 1 ha carbon sampling plots which are periodically measured by researchers associated with the MPOB. The peat soil plantations possess only slightly varying topography (e.g. <1 m vertically over 100 m horizontal distance). The 2 year old palms consisted mainly of fronds with the above-ground stems being negligible. Besides the young palms, the 2 year old plot also contained stacking rows of woody material which were overgrown by vegetation and were higher than the TFH of the palms. The 7 year old plot contained significant undergrowth and the same heaped rows of timber between every other palm row, though here the palms had grown higher than this topographic variation. In the 10 year old plot there was significantly less undergrowth, likely due to light limitation as the fronds of neighbouring palms begin to overlap, as well as a very high water table due to a difference in local topography. Undergrowth here occurred mainly along drainage channels dug between every other palm row.

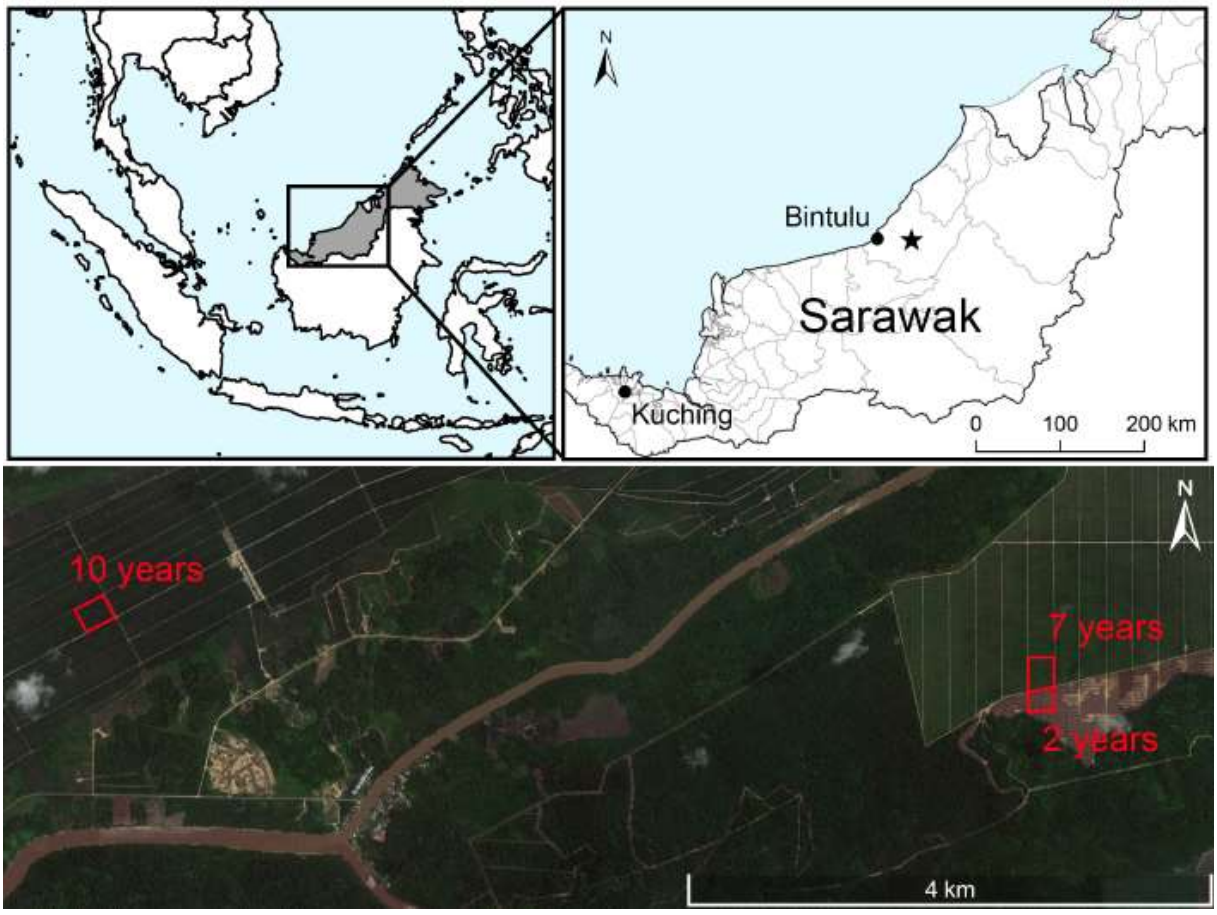

Figure 1: Top: The state of Sarawak in Malaysian Borneo with a star marking the location of the studied plantation (shapefiles from www.diva-gis.org). Bottom: Satellite imagery with the location, extent and age in years of the studied plots (Google Earth).

2.2 Data acquisition

2.2.1 Field sampling

Measurements in the field were conducted on a per-palm basis. Within the boundaries of the existing 1 ha carbon sampling plots, palms were sampled in a grid pattern in accordance with the subdivided squares of the plot. Outside of carbon plots, palms were sampled following a random sampling scheme. 33, 22 and 37 palms were selected for measurement in the 2, 7 and 10 year old plots respectively, with the number of samples varying due to sampling time constraints and accessibility of the plots. TFH as a metric representing canopy height was measured as the distance between the apex of the highest frond and ground level, to provide a validation for SfM photogrammetry derived heights. The stem height was also measured as the distance between the petiole base of the lowest intact frond and ground level (see Morel, Fisher, and Malhi 2012). Due to the size of the older palms, both heights were consistently measured using a laser rangefinder in all plots. These systems typically possess decimetre accuracy.

2.2.2 UAV flights and GPS data

The UAV used for this study was a 3DR Solo quadcopter containing a pixhawk 2.0 flight controller. Including payloads it weighs under 2 kg and is capable of approximately 15 minutes flying time on a single battery. The system was selected due to its ease of use and flexibility. Flights were programmed

in the ArduPilot Mission Planner software by drawing a polygon per plot that was reused for all flights. Flights were conducted at an altitude of 100 m and a speed of 5 m s^{-1}. The minimum frontal and side overlap was defined as 75%. For the 10 year old plot, a replicate was flown using identical flight parameters to enable an independent assessment of the photogrammetric reconstruction and derived parameters as done in previous studies (Dandois et al. 2017). UAV flights were conducted close to solar noon for all acquisitions when lighting conditions are optimal for later photogrammetric reconstruction (Dandois, Olano, and Ellis 2015), and wind speeds at ground level were below 4.5 m s^{-1}. Flight details are summarised in Table 1.

The sensor mounted on the UAV was a consumer-grade RGB camera (Ricoh GRII). The ground sampling distance (GSD) at 100 m altitude was 2.52 cm. The camera was triggered by intervalometer every 2 seconds during the flight – chosen since the flight planning software suggested that this would ensure the desired 75% front and sidelap (with higher effective frontal overlap of 82%), close to the optimal overlap of 80% recommended by Dandois et al., (2015) for vegetation SfM photogrammetry workflows. The focus was set to infinity, white balance to automatic and exposure time (1/1250 s – 1/1600 s) as well as aperture (f2.8-f3.2) and ISO (100-200) were varied based on the illumination conditions and site characteristics (direct/diffuse and amount of shadow) but kept constant throughout each flight, following recommendations from previous studies (Cunliffe, Brazier, and Anderson 2016; O'Connor, Smith, and James 2017).

For georeferencing, a total of 10-15 ground control points (GCPs) and >10 height validation points were surveyed per site using a Trimble Geo 7x GNSS system coupled with a Zephyr Model 2 antenna and were post-processed using RINEX data acquired from the Department of Survey and Mapping Malaysia (JUPEM) to yield 3 cm horizontal and 5 cm vertical precision. These measurements allow SfM photogrammetry generated digital surface models to be adequately constrained (Tonkin and Midgley 2016) and can be used to validate georeferencing accuracies utilising unused GCPs as check-points. GCP distribution followed recommendations from previous work on UAV SfM survey accuracies (James et al. 2017) by ensuring placements around the boundaries of the region of interest as well as close to the centre of each plot.

In addition to the main data acquisition described above, an additional RGB image dataset covering the entirety of the studied 10 year old plantation block was acquired by the Mapping Unit of Sarawak Oil Palms Berhad. The system used was a DJI Phantom 4 with integrated camera, flying at 150 m and 11 m s^{-1} resulting in a GSD of 3.93 cm $pixel^{-1}$. The programmed flight plan was aimed at acquiring image data with 60% frontal and side overlap. This acquisition plan allowed for coverage of one entire plantation block using a single DJI flight battery.

Table 1: List of UAV flights used in this study, referred to by an identifier throughout the remainder of the manuscript and indicating the flight parameters, the palm age plot site (including the replicate for the 10 year old plot) and date of acquisition.

Identifier	**System**	**Sensor**	**Altitude (m above ground level)**	**Speed (m s^{-1})**	**Overlap**	**Site**	**Date**
HO_2yr	3DR Solo	Ricoh GRII	100	5	>75%	2 year	30 January 2018

HO_7yr	3DR Solo	Ricoh GRII	100	5	>75%	7 year	9 February 2018
HO1_10yr	3DR Solo	Ricoh GRII	100	5	>75%	10 year	2 February 2018
HO2_10yr (replicate)	3DR Solo	Ricoh GRII	100	5	>75%	10 year	2 February 2018
LO_10yr	DJI Phantom 4	Integrated camera	150	11	60%	10 year	5 February 2018

2.3 Photogrammetric processing

The photogrammetric processing of UAV-acquired images was performed in Agisoft Photoscan Professional V1.4.2 (St. Petersburg, Russia). There are a number of software options available for photogrammetric processing and Photoscan was selected here due to its successful use in similar applications such as forest inventories (Dandois and Ellis 2013; Puliti et al. 2015), and the ability to use previously developed Python scripts for spatial uncertainty estimation (James, Robson, and Smith 2017). Palms differ considerably from coniferous or broadleaf trees, however no inter-comparison of software options and algorithms exists for this canopy type. Images per flight and plot were input into the software, upon which tie-points within images are identified and used for image matching (algorithms used are proprietary, but a similar method is the scale invariant feature transform (SIFT) algorithm (Lowe 2004)). An automatic aerial triangulation followed by a bundle block adjustment is then performed, reconstructing scene geometry while accounting for camera orientation and distortion. The resulting sparse point cloud representing the tie-points in 3D space is used to generate a rough mesh of the scene. After this initial processing, GCP coordinates are imported and their position manually identified within the images. To evaluate the geometric accuracy of the resulting model, ≈25% of measured GCPs per site were omitted from the photogrammetric processing and used as independent check points. The initial processing was re-run on the highest setting (with key point limit: 80’000, tie point limit: 8000), followed by depth-map and dense point cloud generation on high settings. Depth filtering was disabled as even mild depth filtering appeared to remove points of vertical palm fronds.

While geometric uncertainties of the resulting model are reported by the software (see supplementary information for examples), these only represent errors in relation to the measured GCPs and check points at ground level, which are clearly identifiable within the image. At the top of the canopy, errors can be expected to be considerably larger, as the *z* dimension cannot be adequately constrained by the measured GCPs and values are more heavily dependent on the non-reproducible tie point identification. To quantify the precision of the photogrammetric processing as outlined in aim b), which is impacted by varying camera geometry and GCP uncertainties, we utilised a Monte Carlo (MC) method developed by (James, Robson, and Smith 2017) to derive point precisions representing the expected one standard deviation in *x*, *y* and *z* directions by running many simulations of the sparse point cloud generation including GCP information while randomly varying parameters within reported accuracy thresholds. Precision estimation is performed based on the sparse point cloud as the dense matching does not optimise the image network and, while it can introduce additional smaller errors, does therefore not affect the underlying precision (James, Robson, and Smith 2017). This method was primarily developed for the assessment of SfM based surveys of non-vegetated landforms but the

precision estimates it generates, we argue, can also prove useful for vegetation focused studies. The algorithm was originally designed by (James, Robson, and Smith 2017) for time-series change analysis that accounts for survey-to-survey uncertainties, but can be used stand-alone on single surveys to highlight areas of higher and lower point precision, in 3 dimensions. 1000 simulations proved sufficient, assessed by the difference between the MC means and the initial error free values. Per-point precision estimates in each dimension were generated based on the simulations, using the 'sfm-georef' software (James and Robson 2012).

2.4 Point cloud processing and parameter retrieval

The processing workflow for oil palm segmentation and derivation of TFH and stem height is demonstrated in

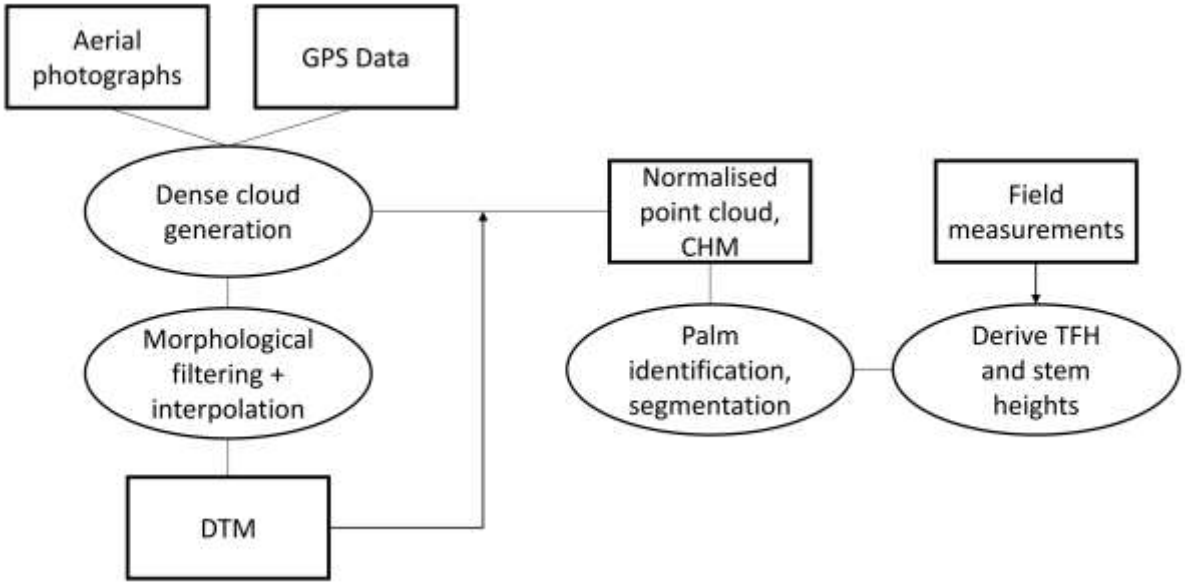

Figure 2. After generating the dense point cloud representing the volumetric structure of the scene, a statistical outlier filtering was performed (CloudCompare, V2.9.1), removing points far above or below the scene which are considered as noise, likely attributed to movements of palm fronds between images. As most scenes contained water, either as standing water or in drainage channels, this caused errors in the photogrammetric processing due to reflections and larger negative outlying point clusters were found, an effect also described by Duffy et al., (2017). The majority of these outliers were removed by eliminating points below a feasible threshold, informed by GCP heights. A minimal amount of manual clipping of the point cloud in CloudCompare (V2.9.1) was therefore required.

Due to the lack of detailed topographical data of the sites, the digital terrain model (DTM) had to be derived from the SfM point cloud. Ground points in each plot were classified by excluding the vegetation through a morphological filtering procedure, originally developed for airborne laser scanning (Zhang et al. 2003) and implemented in the R lidR package (Roussel and Auty 2018). This method has previously been applied for SfM-based DTM generation (Dandois and Ellis 2013) and was selected as it provided more control over the filtering process. It appeared to perform better for sparse ground points as opposed to PhotoScan's own implementation of ground classification which has been used for DTM generation in more recent SfM based studies where more ground information was available (e.g. Cunliffe, Brazier, & Anderson, 2016). It did however require the point cloud to be subsampled with a 0.1 m distance constraint between points for efficient processing. The parameters for morphological filtering had to be adjusted for each plot due to the varying height and density of

palm crowns. The classified ground points were interpolated using k-nearest-neighbour inverse distance weighting. The noise filtered original point clouds were normalised using the derived DTM, yielding height above ground for the remaining vegetation points and canopy height model (CHM). For palm identification, the CHM was first smoothed using a mean filter after which local-maximum filtering was applied with a window size informed by the known planting distance between palms (approx. 9 m, an established planting pattern for oil palm (Chong et al. 2017)). Individual palms were then segmented from the point cloud using a crown delineation method by Silva et al., (2016) and adjusted by Roussel and Auty, (2018), using the identified palm points as centroids and the CHM as input. This particular delineation method was selected due to its suitability for the simple circular footprint of oil palm crowns and as the impact of overlapping fronds can be reduced by constraining the buffer radius used. Other methods based on watershed analysis or region-growing (Dalponte and Coomes 2016) proved to have issues where overlap occurred.

The TFH values for each segmented palm were retrieved by selecting the maximum point within the cloud, the sensitivity to erroneous outliers reduced by the previous statistical outlier filtering. Derived TFH is assessed against field measured TFH for measured palms. To test the consistency of TFH for two independent builds, TFH was also derived from a replicate dataset over the 10 year old plot and the values compared for the same palms.

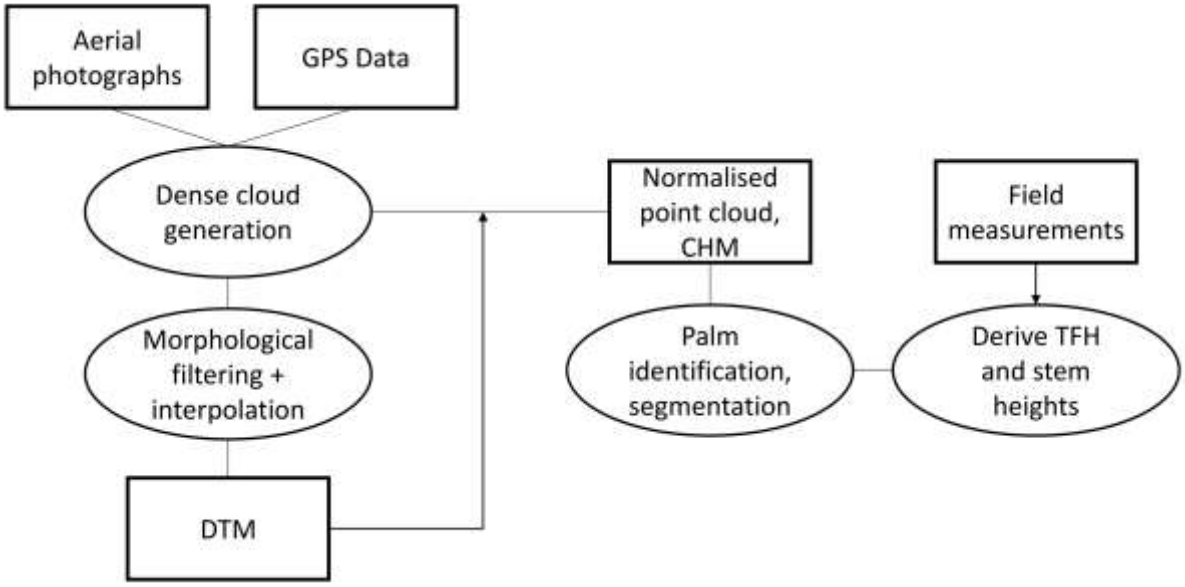

Figure 2: Processing workflow for deriving per-palm height metrics from UAV data.

Using linear regression, the correlations of different height percentiles (30 to 90% in 10% steps), and the mean and maximum point height with field measured stem height were assessed for the samples of the 7 and 10 year old plantation. For the 2 year old palms, the bases of the lowest intact fronds were at ground level and therefore no stem was measured. Due to a limited number of samples, prediction accuracy was assessed using leave-one-out cross validation (LOOCV) as used in similar studies (Wang Li et al. 2016). Two separate models depending on plot age were assessed as the relationship between point cloud metrics and stem heights can be expected to differ slightly between palms of different age classes. This does not avoid the issue of younger, re-planted palms within the same plots. The relationships with highest coefficient of determination (R^2) were then applied to all identified palm point clouds to derive stem heights.

3 Results

3.1 Photogrammetric dense clouds

UAV image data averaged around 350 images per plot and acquisition, from which dense point clouds were generated for each plot through photogrammetric processing. For the 10 year old plot, a replicate dataset using the same acquisition parameters was generated (HO2_10yr), as well as a coarser resolution sparser dataset for the entire plantation block (LO_10yr).

Subsets of the point clouds from the three different aged plots are displayed in Figure 3. Initial visual inspections of the generated dense point clouds per plot show reconstructions of individual palm fronds. Noise increased for higher, more vertically-oriented fronds. The point density decreased towards the apical stem as fronds overlapped more. No information on the trunk was captured as it was entirely obscured by fronds in all images. The 10 year old plot contained fewer points from the ground and bottom fronds due to the high canopy density.

Figure 3: RGB dense point cloud subsets (33x33 m) of the 2, 7 and 10 year old plantation datasets, resulting from the HO_2yr, HO_7yr and HO1_10yr flights.

The geometric accuracies of the scene reconstructions, assessed by check points which were not used for the photogrammetric processing (≈25% of total GCPs per site), were high with mean horizontal errors (*x*, *y*) of 2.29 cm and mean vertical errors (*z*) of 3.4 cm (see supplementary information for individual processing reports).

The LO_10yr dataset showed significantly lower point density (a 1 ha square extracted from the dense clouds contained 10.26 Mio points for HO1_10yr and 1.69 Mio points for LO_10yr) but still appeared to represent finer details and individual fronds of single palms. At the higher altitude and speed of this flight, surface points were imaged 8 times and the ground resolution was 3.93 cm per pixel (for HO1_10yr, points were imaged 44 times on average at 2.52 cm per pixel). The average of 8 images per ground point indicates that the overlap lies slightly below the targeted 60% recommended for photogrammetric surveys (Dandois, Olano, and Ellis 2015). This may have been due to acquisition conditions on the day of the flight, or imperfect flight planning.

Geometric accuracies reported by check points for LO_10yr were lower than the other flights with horizontal error (*x*, *y*) of 12.9 cm and vertical error (*z*) of 39.1 cm.

For the generation of maps from the sparse point cloud precision estimates, values were interpolated for the dense point locations using nearest-neighbour inverse distance weighting. It should be noted that due to the reduced overlap for LO_10yr, there were considerably fewer tie points within the sparse point cloud (Table 2, see supplementary information for visual representations). The resulting map therefore includes a higher amount of interpolation and the precision estimates are more poorly resolved spatially. Derived statistics should be treated with caution as there can be expected to be a bias depending on the 3D location of tie points identified during processing, such as a lesser proportion of points found inside the vegetation canopy.

The mean precisions do not exhibit large differences between low and high overlap acquisitions. Horizontal precisions in *x* and *y* were very slightly larger for HO1_10yr, while vertical precisions (*z*) are slightly lower on average (Table 2). When displaying point precisions spatially (

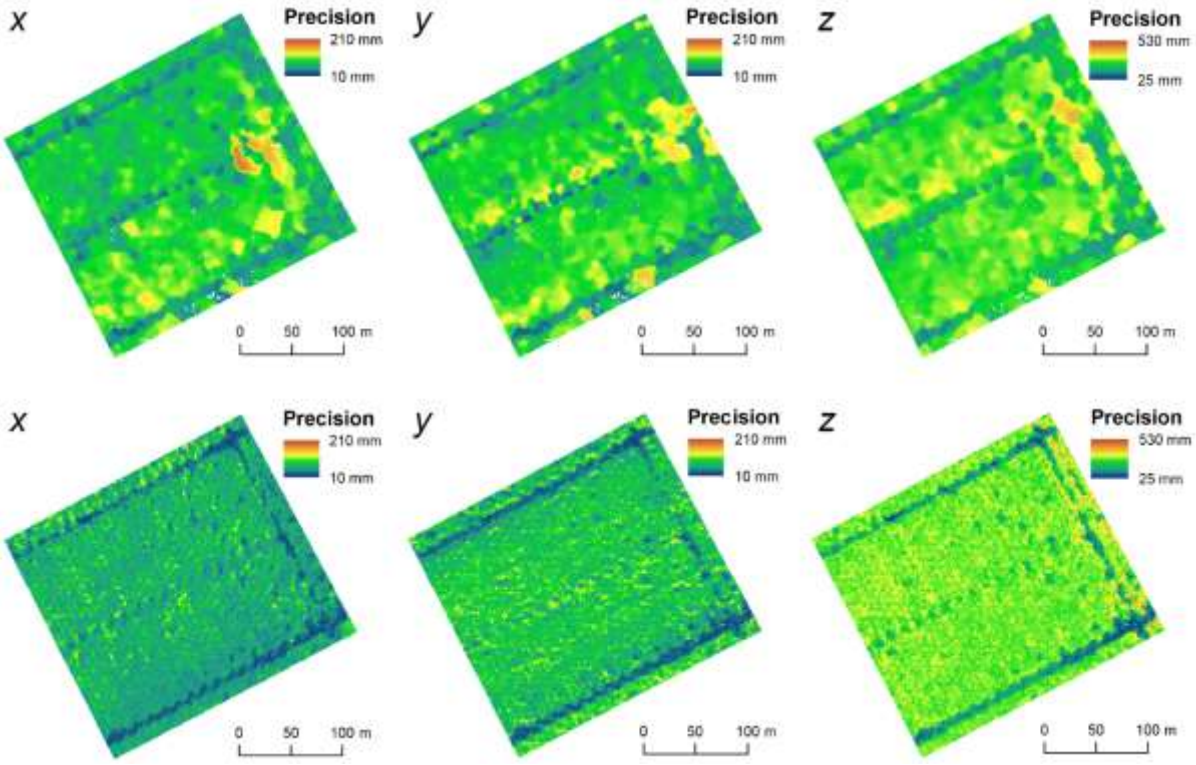

Figure 4: Maps of interpolated point precisions in x, y and z direction for the 10 year old palm plot. Top row: Acquisition with 3.93 cm pixel^{-1} GSD and 60% nominal overlap (LO_10yr). Bottom row: Acquisition with 2.52 cm pixel^{-1} GSD and 75% nominal overlap (HO1_10yr).

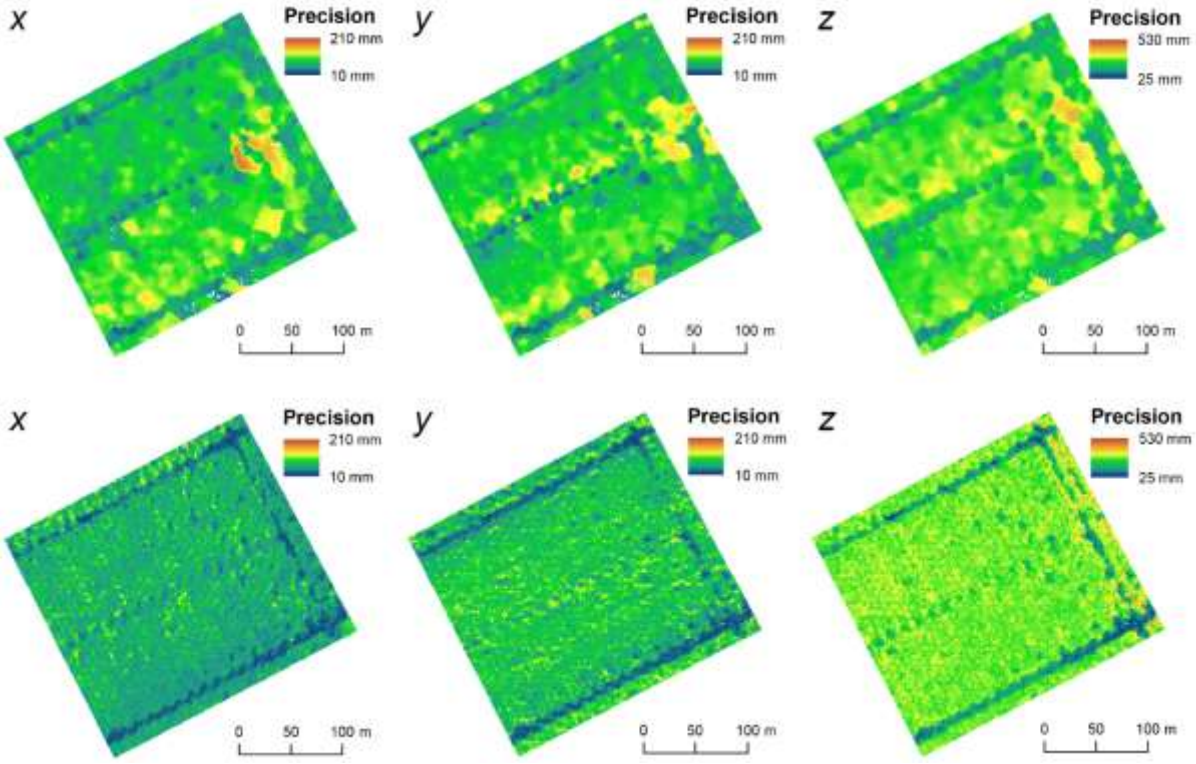

Figure 4), it is apparent that precisions are higher for the flat ground surface on which GCPs were placed as opposed to points located vertically above the ground, within the vegetation canopy.

LO_10yr displays larger patches of lower precision, due to the sparser tie points. Such patches of low precision may influence the reliability of the derived DTM. For HO1_10yr, precisions are higher for resolved ground points. Vertical precisions appear lower but more uniform for the vegetation canopy, with some edge effects at the north-eastern border.

Table 2: Parameters for the two different acquisitions over the 10 year old plot along with mean precision estimates in *x*, *y* and *z* directions.

Acquisition overlap	GSD (cm pixel^{-1})	Tie point density (points m^{-2})	Mean *x* precision (mm)	Mean *y* precision (mm)	Mean *z* precision (mm)
<60%	3.93	0.05	77.35	89.86	247.90
>75%	2.52	10.28	68.34	80.29	267.39

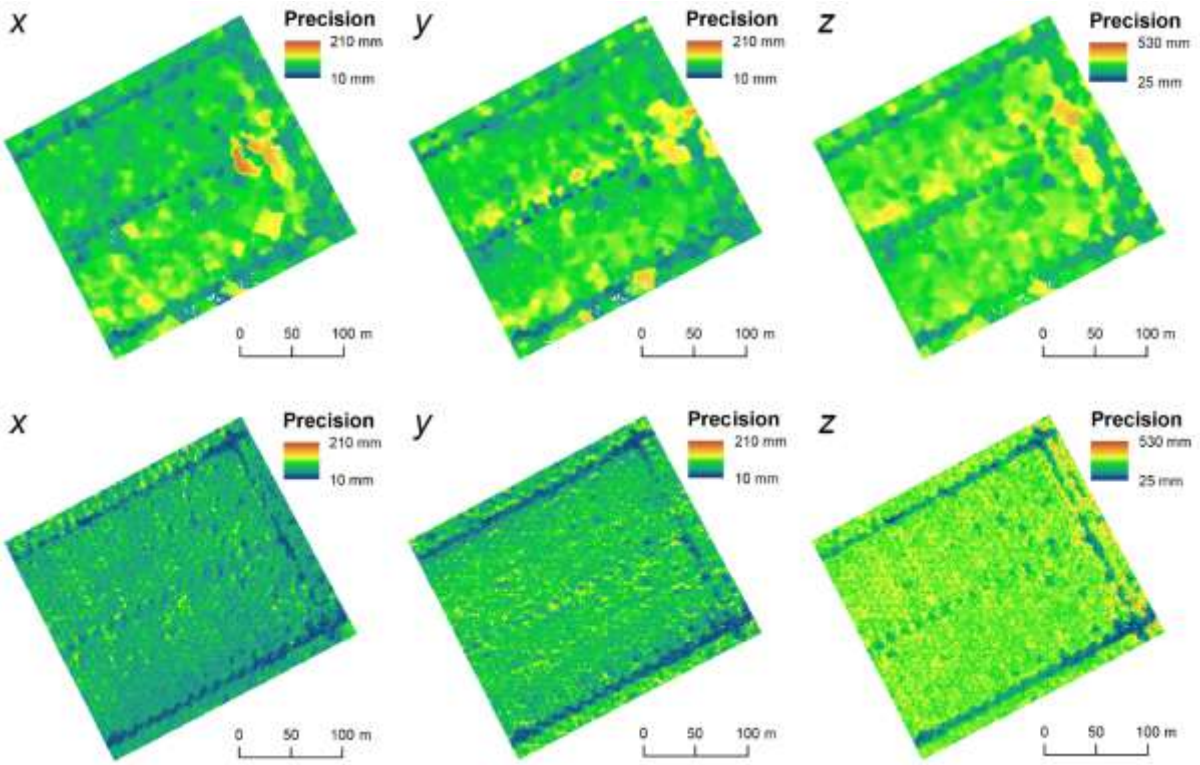

Figure 4: Maps of interpolated point precisions in *x*, *y* and *z* direction for the 10 year old palm plot. Top row: Acquisition with 3.93 cm pixel^{-1} GSD and 60% nominal overlap (LO_10yr). Bottom row: Acquisition with 2.52 cm pixel^{-1} GSD and 75% nominal overlap (HO1_10yr).

3.2 Digital terrain models

After filtering out non-ground points the remaining points were interpolated to derive a DTM per site. The DTM accuracy was assessed using height validation points measured between palms in the field

with reported mean measurement horizontal precisions of 3.23 cm and vertical precisions of 5.74 cm. Mean vertical absolute errors assessed for height validation points were 9.1 cm for the 2 year old (HO_2yr), 12.4 cm for the 7 year old (HO_7yr) and 12.12 cm for the 10 year old plot (HO1_10yr). LO_10yr resulted in errors of 31.62 cm. The increase in errors from the 2 year old to the older plots is due to less visible ground within the imagery and thus non-uniformly distributed ground points within the dense cloud. For the 2 and 7 year old plots, DTM heights were generally over-estimated (Figure 5). This overestimation is assumed to be related to undergrowth which obscures the ground beneath. While there is very little undergrowth present in the 10 year old plot, the reason for the underestimation of ground height is unclear but likely due to interpolation related uncertainties as well as the larger amount of drainage channels in this plot.

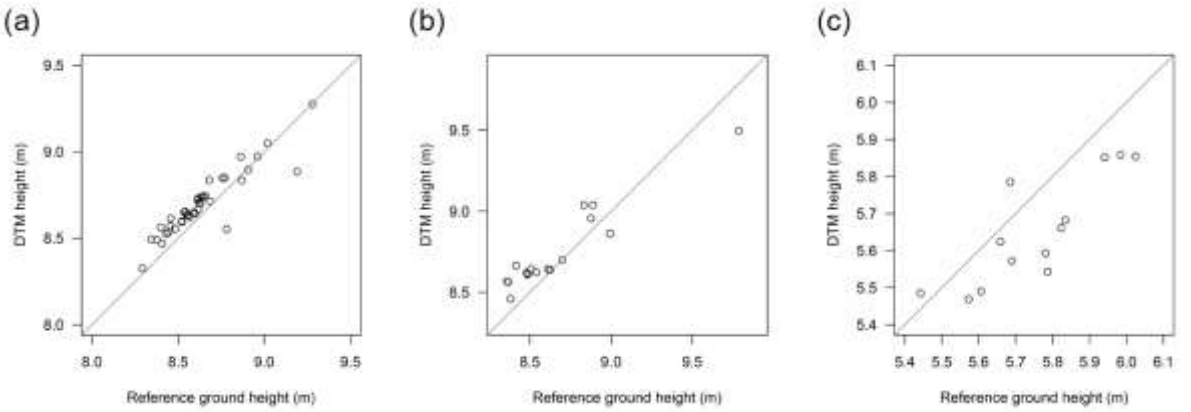

Figure 5: Interpolated DTM heights above mean sea-level versus GPS measured reference ground heights. (a): 2 year old plot, (b): 7 year old plot, (c): 10 year old plot.

3.3 Palm identification

The local maximum palm identification algorithm performed relatively well for the 7 and 10 year old palm plots (containing 776 and 654 palms total), with a mapping accuracy (MA: correctly identified/(true total + commissions)) of 98.2% and 94.9% respectively. The identified palm locations for the 10 year old plot derived from HO1_10yr are illustrated in

Figure 6, along with a subset showing an example of omitted palms. For the 2 year old plot, this method caused a large amount of omission and commission errors in the vicinity of the overgrown stacks of woody material between the palm rows, as the vegetation here was higher than the palm canopies. Neglecting these stacks and immediately adjacent palms, the method showed a MA of 80.4% for 238 palms total.

The MA for the same region of the 10 year old plot using LO_10yr is 94.0%.

Figure 6: Left: Resulting palm locations (yellow points) for the 10 year old plot and subset location (white rectangle), right: Subset illustrating omitted palms (red circles).

3.4 Height metrics

Maximum values of the individual palm point clouds were assessed against the TFH measured in the field. Results showed relatively large deviations between TFH measurements and maximum point cloud values with mean absolute errors of 0.383 m for HO_2yr, 0.968 m for HO_7yr and 1.246 m for

HO1_10yr, which represented 18.9%, 13.7% and 11.7% of the mean measured heights respectively (Figure 7). LO_10yr showed lower mean absolute errors of 1.099 m for TFH of the 10 year old plot.

When comparing the maximum values between the replicates HO1_10yr and HO2_10yr for the field measured palms (**Error! Reference source not found.**), this resulted in a mean absolute error of 0.199 m. Deviations between the values appear independent of field-measured height. One obvious outlier is visible, caused by overlap resulting in a different segmentation of the palm. The magnitude of this deviation between replicates is consistent with values generated by the MC point precision analysis on the sparse point cloud (Table 2).

To establish the optimal metrics for deriving stem height from the point cloud it was necessary to establish separate linear relationships between basic point cloud height metrics of the segmented palm point clouds and the structural metric of stem height using LOOCV for different age stands (Table 3). For the 2 year old plot, the stem height above ground was negligible and so is not analysed. The strongest relationships (according to R^2 values) with stem heights of the 7 year old plot was shown by the maximum value (R^2 = 0.63; Table 3), while for the 10 year old plot the 80th percentile of elevations performed better (R^2 = 0.69; Table 3). The MAEs represent 12.2% and 30.9% of mean stem heights respectively. Results for the low overlap acquisition showed overall lower R^2 values compared to the high overlap dataset, but was consistent in showing the best relationship for the 80th elevation percentile (R^2 = 0.59).

Using these linear models to derive stem heights from the extent of each plot (i.e. using heights derived from the UAV-SfM derived point clouds) for the 7 and 10 year old plots yields the distributions in Figure 9. For the 7 year old plot, negative values for predicted stem heights were constrained to 0 which results in high counts for this bin. Despite the errors introduced, these models coupled with the segmented point cloud represent an efficient method for the mapping of stem height and thus provides necessary information for spatially differentiated AGB and carbon retrieval. Fine-grained remotely sensed data thus enables single palm based estimates over spatial extents which would require immense efforts of field-based sampling.

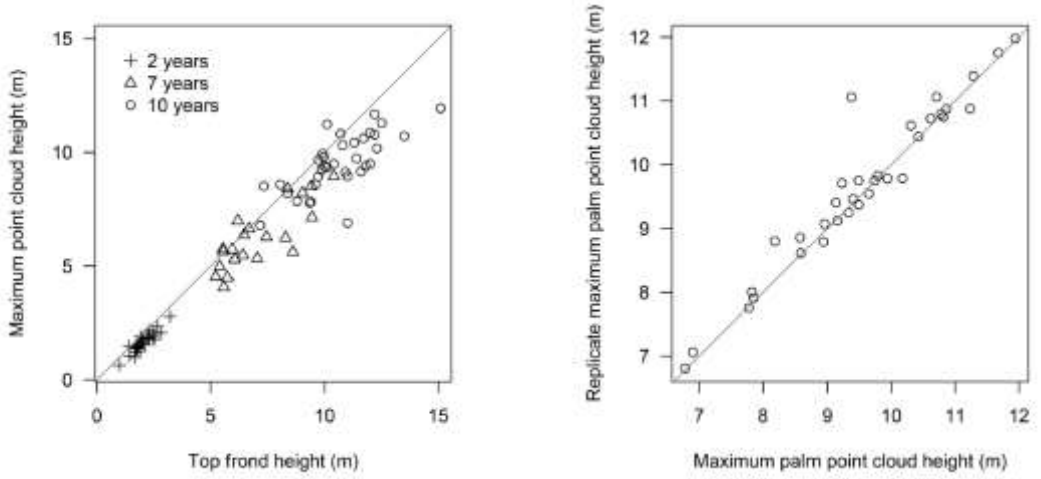

Figure 7: Maximum point cloud heights plotted against field measured TFHs for 2 year, 7 year and 10 year old palms.

Figure 8: Maximum point cloud height compared for the same palms between replicates of the 10 year old plot.

Table 3: Linear stem height model strength, root-mean-square errors (RMSE) and mean absolute errors (MAE) for the 30th - 90th point cloud height percentiles as well as the maximum and mean values. Reported for the 7 year old plot and the 10 year old plot with high and low overlap acquisitions. The highlighted rows show the models with the highest R^2 values which are used subsequently for stem height estimation.

	HO_7yr, *n* = 22			**HO1_10yr, *n* = 37**			**LO_10yr, *n* = 37**		
Percentile	R^2	RMSE (m)	MAE (m)	R^2	RMSE (m)	MAE (m)	R^2	RMSE (m)	MAE (m)
30%	0.56	0.30	0.24	0.64	0.48	0.40	0.52	0.50	0.42
40%	0.62	0.28	0.21	0.64	0.48	0.40	0.54	0.49	0.41
50%	0.61	0.28	0.21	0.64	0.48	0.39	0.55	0.48	0.39
60%	0.60	0.29	0.21	0.66	0.47	0.38	0.55	0.49	0.38
70%	0.58	0.29	0.21	0.68	0.45	0.36	0.54	0.49	0.38
80%	0.58	0.29	0.22	**0.69**	**0.45**	**0.34**	**0.59**	**0.46**	**0.37**
90%	0.57	0.30	0.22	0.68	0.45	0.34	0.57	0.47	0.38
Max	**0.63**	**0.27**	**0.22**	0.52	0.55	0.39	0.41	0.56	0.45
Mean	0.61	0.28	0.21	0.48	0.58	0.43	0.54	0.49	0.39

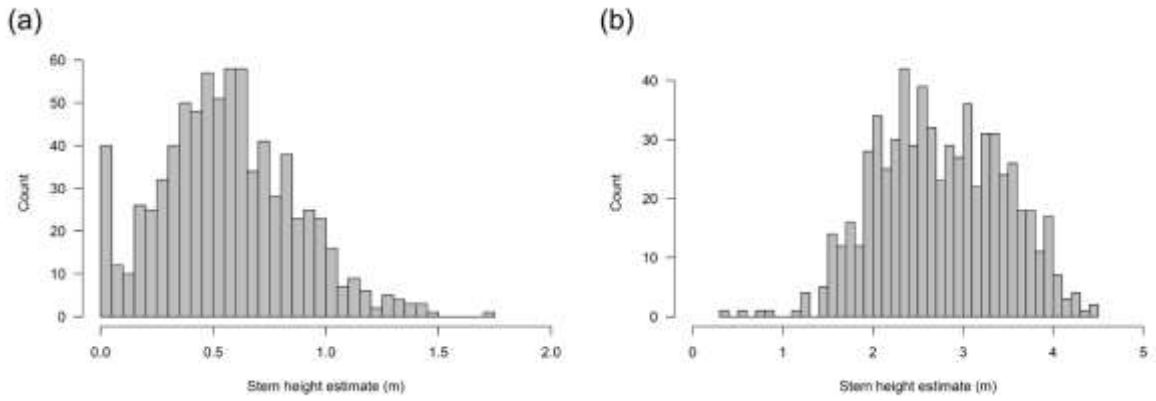

Figure 9: Histograms of estimated stem heights for the 7 year old plot (a) and 10 year old plot (b).

4 Discussion

This manuscript has presented an operational processing workflow for deriving per-palm height metrics from UAV image data while quantifying method-inherent uncertainties introduced at different stages. As demonstrated, it is possible to successfully segment single palms from fine-grained, UAV-derived SfM based datasets and derive TFH and stem height from point-cloud-derived products. Subsequent sections of this discussion will address precision estimates and accuracies of the generated results, and their implications for the application of this method in management and research of oil palm plantations.

4.1 Uncertainties within resulting SfM point clouds

Uncertainties resulting from SfM processing were estimated using a method which has not previously been applied to a vegetation focused study. If correctly parameterised, this method may reduce the need for time consuming replicates from independent acquisitions which are commonly advocated in SfM based studies (Dandois et al. 2017; Dandois, Olano, and Ellis 2015). Overall, the precision maps provide a better spatial indication of the SfM method's inherent uncertainties than relying exclusively on values reported by GCPs and check points as a measure of reconstruction quality, which due to the limited number of surveyed GCPs and the lack of GCPs at canopy level cannot adequately represent uncertainties across the scene. However, it must be noted that these precision maps can't account for some systematic errors (e.g. doming) and do not represent accuracy, which can only be assessed using check points (James, Robson, and Smith 2017). Sparse point precisions at ground level were higher (<10 cm) than for the vegetation canopy (20-50 cm). The contrast between precisions of the lower (60%) versus higher (>75%) overlap acquisition highlighted that ground information resulting from higher overlap flights appears more reliable, an observation which has previously been made for forested areas (Dandois, Olano, and Ellis 2015). These uncertainties were confirmed at the dense point cloud level by comparing per palm maximum values from a replicate dataset.

4.2 Quality of derived DTMs

Retrieving accurate ground elevations from SfM can introduce considerable uncertainties but doing so represents an alternative to time consuming manual surveys when lacking LiDAR coverage of the studied area, for point cloud normalisation and CHM determination. We found that undergrowth caused an overestimation of the elevation of identified ground points, while dense canopies led to the absence of information about the ground position. Interpolating between sparse ground points as was required in this study for the 10 year old plantation was only feasible for regions of very slightly varying topography as is the case for peat-soil plantations which show very subtle changes in topography at landscape extents (Ballhorn, Jubanski, and Siegert 2011). Although the MAE of the measured ground points did not exceed 20 cm for all the studied areas, it can be expected that uncertainties in the DTM remain a major limiting factor in the quality of resulting canopy height metrics. An increase in DTM error resulting from fewer ground points was observed for the lower overlap (60%) acquisition, suggesting that higher overlap is recommended if DTMs must be derived from SfM point clouds alone.

4.3 CHM-based palm identification

Local maxima based palm identification informed by planting distance performed very well (98.2% MA) for palms of intermediate ages (here 7 years), when they were taller than surrounding vegetation and other topographic variations (e.g. mounds of overgrown timber) and when their fronds did not yet overlap by more than a few decimetres. This mapping accuracy is identical to that reported by Kattenborn et al., (2014) for dense palm stands without overlap. The performance of height based identification of young palms (2 years) was heavily dependent on the plantation structure and undergrowth. Excluding areas with large local topographic variations our approach performed moderately well with 80.4% mapping accuracy, influenced predominantly by false positives from tall undergrowth. In the plot studied here, the application of the method to the entire plot was complicated by the overgrown stacks of organic material which resulted in false positives and

sometimes obscured adjacent young palms. We advise that local maximum methods are not appropriate for direct application to plantation blocks with such topographic variations. For older plantations (10 years), the resulting MA of 94.9% was caused by issues with overlap and smaller palms which are surrounded by taller ones not being identified as local maxima. This could be partly addressed by decreasing the window size of the local maximum filtering, which would however introduce more false positives.

4.4 Assessing maximum point cloud height against TFH

Comparing the maximum point cloud height with field-measured TFH appeared to show a high uncertainty but also an apparent negative bias for the UAV-derived metric (Figure 7). The large deviations between field measurements and point cloud metrics are likely due to biases also in field measurements – e.g. including the manual identification of the highest frond, selection of its highest part and a possible *x*, *y* discrepancy between the reference point on the ground and the highest measured frond point. Treating the field validation data as a perfect baseline against which to assess the SfM result is probably a flawed approach, and both datasets should be considered as uncertain. This difficulty of validating SfM-derived height metrics for higher vegetation such as trees has also been encountered in previous studies (Lisein et al. 2013). Here this issue is not solved but addressed by the generation of tie-point precision estimates which provide further insight into the method-inherent uncertainties, which we show to be relatively low (e.g. < 10 cm) for ground points and higher at canopy level, averaging around 30 cm as visible in

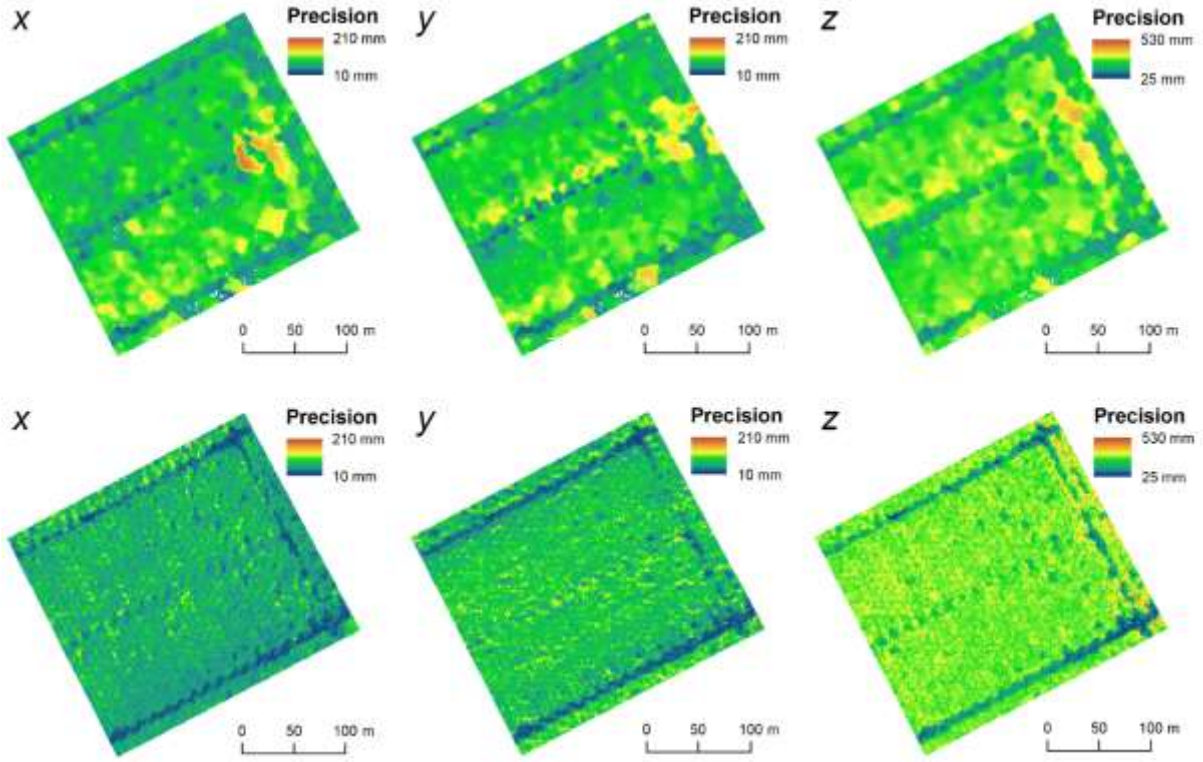

Figure 4.

The negative bias apparent in the results (Figure 7) is expected to be independent of the above uncertainties and can be partially explained by the effect of undergrowth on the interpolated DTM surface. For the 10 year old palm plot this is however not consistent with height validation measurements where the DTM values were below the reference. Further bias may originate from an inherent smoothing effect of the dense matching process, observed in previous studies where SfM

point clouds were compared to LiDAR reference data (Lisein et al. 2013), but this is contradictory to the fact that LO_10yr produced maximum height values closer to field measured TFH.

Overall, the errors resulting for the TFH (or top-of-canopy height) estimation are very close to those reported by other studies applying SfM methodologies to vegetated systems of similar height range (Wallace et al. 2016; Panagiotidis et al. 2017). Better results can be achieved when employing a LiDAR-derived DTM (Lisein et al. 2013; Puliti et al. 2015), though this represents a considerable operational constraint. The inclusion of convergent imagery at non-nadir angles (e.g. 45°) has also been advocated as besides strengthening the image network for reconstruction it can result in more ground points being visible to aid in DTM generation (Cunliffe, Brazier, and Anderson 2016). The latter aspect may be negligible for dense canopy cover but could yield better results for younger palms. The impact on point precisions and DTM error would benefit from further study, especially in relation to the cost of additional acquisitions and processing time.

4.5 Point cloud height metric based stem height estimation

Assessing the relationship between different point cloud height metrics and field measured stem height did not show very large differences between the metrics used. Nevertheless, the strongest relationship differed between the two different aged plots analysed, which can likely be attributed to different point cloud characteristics as a result of canopy density. For 7 year old palms where little to no overlap occurs, a greater portion of the fronds were resolved in the point cloud; while for the 10 year old palms the lower fronds were completely, or partially obscured. When applying the resulting models to generate estimates of stem height distributions throughout the plots, it is striking that there were relatively large value ranges for plots of the same age, considerably larger than the resulting MAEs. For the 7 year old plot, there were however a considerable number of negative values, which were re-set to zero for the analysis. The two primary causes for this were local DTM errors caused by undergrowth as well as the fact that younger, later planted replacement palms have significantly smaller fronds which results in under-estimation of stem height by the linear model. Due to the amount of palms affected, we advise that a solution should be sought before applying this model for stem height estimations. Given a large amount of field samples across multiple palm ages, it may be possible to identify a robust non-linear relationship which accounts for age-dependent differences. This would allow efficient and accurate retrieval of per-palm trunk biomass from SfM point cloud data using allometric equations, given assumptions about diameter at breast-height (DBH) (Corley and Tinker 2016).

4.6 Implications for oil palm plantation management and research

The methods for palm identification, TFH and stem height retrieval presented here are applicable to image data from consumer grade UAV systems, provided such data are acquired with sufficient spatial overlap. Our workflow can thus be of relevance to improved plantation management – because it can deliver maps indicative of plantation status at relatively low financial cost. Repeat acquisitions would further allow the identification of height increments over time and local variations in height could possibly be correlated with oil palm yield, for example by influencing the light regime (Corley and Tinker 2016). The retrieval of height metrics appears to work almost as well for lower resolution, lower overlap acquisitions (LO_10yr) as they do for acquisitions focused on retrieving a higher quality point cloud (e.g. HO1_10yr). This is an important insight when seeking to maximise the spatial coverage of

survey flights, whilst also reducing the time required for acquisitions and data processing. A constraining factor regarding both time and cost of UAV acquisitions, following the survey designs presented here, is the reliance on high precision GCP measurements. If the absolute geographic locations are not a necessity, an alternative may be the use of a total station to measure distances between markers. The installation of adequately spaced permanent GCPs would also greatly facilitate repeat acquisitions. Furthermore, with the ongoing development of UAVs that will, in future, carry on-board real-time kinematic GNSS capabilities, immediate high precision georeferencing of the acquired data may become an operational option in the future, minimising the need for ground control (Turner, Lucieer, and Wallace 2014).

The demonstrated usefulness of even low overlap acquisitions to derive height metrics and the increased application of UAVs for plantation management means that there may be an untapped data source of interest for research and a potential for a closer collaboration between researchers and innovative palm oil companies. Despite similar results for HO1_10yr and LO_10yr it can be assumed that for deriving information on younger palm canopies and for finer scale structural information such as frond rachis length and number, utilizing advanced point cloud metrics, higher overlap and finer resolution are required. The ability to derive advanced metrics with higher reliability may also prove useful in predicting per palm biomass, given adequate training and validation data derived from destructive harvesting or estimated AGB derived from allometric measurements of stem height, DBH, petiole cross-section and frond number in the field (Corley and Tinker 2016). Coupled with further concurrent field sampling efforts, UAV SfM photogrammetry derived metrics may be robust enough to provide much needed information to address one aspect of the lack of data for oil palm carbon stock estimates and the impact of the conversion of different land cover to oil palm plantations (Kho and Jepsen 2015).

Emerging work by Malek et al. (2014) and Manandhar, Hoegner, and Stilla (2016) indicates the potential of computer vision and object based detection for automated oil palm identification and counting. Further work is needed to develop and demonstrate the robustness of these methods in complex plots with larger undergrowth. It stands to reason that object based and height based detection possess a number of contrasting advantages and that a hybrid approach including height information and image-based segmentation may yield the most accurate solution. As a DSM typically results from the workflow for orthomosaic generation, no additional data acquisition is required. Therefore this would be a promising direction for future research aiming at developing palm identification methods with sufficient accuracy for commercial application.

5 Conclusions

This study demonstrated the use of SfM point clouds derived from UAV imagery for the identification of single palm canopies and the retrieval of basic structural information based on height metrics from segmented palms. In plantation plots with flat topography as studied here a DTM interpolated from classified SfM ground points proved sufficiently accurate (~10 cm for high overlap acquisitions) for height based studies of oil palm without requiring LiDAR based information, which is key for the operational implementation at similar sites. Employing an MC approach for generating point cloud precision estimates allowed a spatially resolved assessment of SfM data quality which can be used to inform a quantitative assessment of point cloud robustness and suitability for vegetation structure related studies. Local maximum methods for CHM based palm identification performed best for intermediate palm ages (7 years) but show more errors where large undergrowth and overlapping between palm canopies is common. Further it was shown that reliable inventories of the number of palms per plantation block could be generated with acquisition plans which favour coverage over high

overlap, which provides an important benchmark for applying this methodology while maximising the efficiency of data acquisition. However, more highly resolved per-palm point clouds allowed for better estimation of stem height using height percentiles, and enabled the generation of stem height distributions for the studied plots. Due to the amount of detail resolved, it can be assumed that more complex point cloud based metrics could be identified which correlate with other aspects of palm structure and therefore warrant further research. These derived per-palm metrics, besides giving detailed information on plantation status, may prove useful for predicting per-palm AGB and ultimately mapping oil palm carbon stocks, providing an affordable and widely applicable method for carbon accounting.

6 Acknowledgements

This project has received funding from the European Union's Horizon 2020 research and innovation programme under the Marie Skłodowska-Curie grant agreement No 721995. We would like to thank Sarawak Oil Palms Berhad for providing the sites and resources necessary for this study, especially the Geo-Information Department for providing UAV data. Furthermore, we acknowledge the support of the Malaysian Palm Oil Board and its research technicians in providing site assistance and fieldwork help during our measurement campaign.

7 Declaration of interest statement

The authors declare no conflicts of interest.

8 References

Ballhorn, Uwe, Juilson Jubanski, and Florian Siegert. 2011. "ICESat/GLAS Data as a Measurement Tool for Peatland Topography and Peat Swamp Forest Biomass in Kalimantan, Indonesia." *Remote Sensing* 3 (9): 1957–82. doi:10.3390/rs3091957.

Butler, Rhett A., and William F Laurance. 2009. "Is Oil Palm the next Emerging Threat to the Amazon?" *Tropical Conservation Science* 2 (1): 1–10. doi:papers2://publication/uuid/5F4271A6-E2C2-4771-9248-7C5BC701B38B.

Carlson, Kimberly M., Lisa M. Curran, Gregory P. Asner, Alice McDonald Pittman, Simon N. Trigg, and J. Marion Adeney. 2012. "Carbon Emissions from Forest Conversion by Kalimantan Oil Palm Plantations." *Nature Climate Change* 3 (3): 283–87. doi:10.1038/nclimate1702.

Cheng, Yuqi, Le Yu, Yidi Xu, Hui Lu, Arthur P. Cracknell, Kasturi Kanniah, and Peng Gong. 2018. "Mapping Oil Palm Extent in Malaysia Using ALOS-2 PALSAR-2 Data." *International Journal of Remote Sensing* 39 (2): 432–52. doi:10.1080/01431161.2017.1387309.

Chong, Khai Loong, Kasturi Devi Kanniah, Christine Pohl, and Kian Pang Tan. 2017. "A Review of Remote Sensing Applications for Oil Palm Studies." *Geo-Spatial Information Science* 20 (2): 184–200. doi:10.1080/10095020.2017.1337317.

Corley, R. Hereward V., and P. Bernard Tinker. 2016. *The Oil Palm*. 5th ed. Chichester, UK: Wiley Blackwell.

675 Cunliffe, Andrew M., Richard E. Brazier, and Karen Anderson. 2016. “Ultra-Fine Grain Landscape-
676 Scale Quantification of Dryland Vegetation Structure with Drone-Acquired Structure-from-
677 Motion Photogrammetry.” *Remote Sensing of Environment* 183: 129–43.
678 doi:10.1016/j.rse.2016.05.019.

679 Dalponte, Michele, and David A. Coomes. 2016. “Tree-Centric Mapping of Forest Carbon Density
680 from Airborne Laser Scanning and Hyperspectral Data.” *Methods in Ecology and Evolution* 7
681 (10): 1236–45. doi:10.1111/2041-210X.12575.

682 Dandois, Jonathan P., Matthew Baker, Marc Olano, Geoffrey G. Parker, and Erle C. Ellis. 2017. “What
683 Is the Point? Evaluating the Structure, Color, and Semantic Traits of Computer Vision Point
684 Clouds of Vegetation.” *Remote Sensing* 9 (4): 1–20. doi:10.3390/rs9040355.

685 Dandois, Jonathan P., and Erle C. Ellis. 2013. “High Spatial Resolution Three-Dimensional Mapping of
686 Vegetation Spectral Dynamics Using Computer Vision.” *Remote Sensing of Environment* 136:
687 259–76. doi:10.1016/j.rse.2013.04.005.

688 Dandois, Jonathan P., Marc Olano, and Erle C. Ellis. 2015. “Optimal Altitude, Overlap, and Weather
689 Conditions for Computer Vision Uav Estimates of Forest Structure.” *Remote Sensing* 7 (10):
690 13895–920. doi:10.3390/rs71013895.

691 Duffy, James P., Andrew M. Cunliffe, Leon DeBell, Chris Sandbrook, Serge A. Wich, Jamie D. Shutler,
692 Isla H. Myers-Smith, Miguel R. Varela, and Karen Anderson. 2017. “Location, Location, Location:
693 Considerations When Using Lightweight Drones in Challenging Environments.” *Remote Sensing
694 in Ecology and Conservation*, 7–19. doi:10.1002/rse2.58.

695 Fitzherbert, Emily B., Matthew J. Struebig, Alexandra Morel, Finn Danielsen, Carsten A. Brühl, Paul F.
696 Donald, and Ben Phalan. 2008. “How Will Oil Palm Expansion Affect Biodiversity?” *Trends in
697 Ecology and Evolution* 23 (10): 538–45. doi:10.1016/j.tree.2008.06.012.

698 Germer, Jörn, and Joachim Sauerborn. 2008. “Estimation of the Impact of Oil Palm Plantation
699 Establishment on Greenhouse Gas Balance.” *Environment, Development and Sustainability* 10
700 (6): 697–716. doi:10.1007/s10668-006-9080-1.

701 James, Mike R., and Stuart Robson. 2012. “Straightforward Reconstruction of 3D Surfaces and
702 Topography with a Camera: Accuracy and Geoscience Application.” *Journal of Geophysical
703 Research: Earth Surface* 117 (3): 1–17. doi:10.1029/2011JF002289.

704 James, Mike R., Stuart Robson, Sebastian D’Oleire-Oltmanns, and Uwe Niethammer. 2017.
705 “Optimising UAV Topographic Surveys Processed with Structure-from-Motion: Ground Control
706 Quality, Quantity and Bundle Adjustment.” *Geomorphology* 280: 51–66.
707 doi:10.1016/j.geomorph.2016.11.021.

708 James, Mike R., Stuart Robson, and Mark W. Smith. 2017. “3-D Uncertainty-Based Topographic
709 Change Detection with Structure-from-Motion Photogrammetry: Precision Maps for Ground
710 Control and Directly Georeferenced Surveys.” *Earth Surface Processes and Landforms* 42 (12):
711 1769–88. doi:10.1002/esp.4125.

712 Kattenborn, Teja, Maximilian Sperlich, Kataebati Bataua, and Barbara Koch. 2014. “Automatic Single
713 Palm Tree Detection in Plantations Using UAV-Based Photogrammetric Point Clouds.”
714 *International Archives of the Photogrammetry, Remote Sensing and Spatial Information Sciences
715 - ISPRS Archives* 40 (3): 139–44. doi:10.5194/isprsarchives-XL-3-139-2014.

716 Kho, Lip Khoon, and Martin Rudbeck Jepsen. 2015. “Carbon Stock of Oil Palm Plantations and Tropical
717 Forests in Malaysia: A Review.” *Singapore Journal of Tropical Geography* 36 (2): 249–66.
718 doi:10.1111/sjtg.12100.

719 Koh, Lian P., Jukka Miettinen, Soo C. Liew, and Jaboury Ghazoul. 2011. “Remotely Sensed Evidence of
720 Tropical Peatland Conversion to Oil Palm.” *Proceedings of the National Academy of Sciences* 108
721 (12): 5127–32. doi:10.1073/pnas.1018776108.

722 Koh, Lian P., and David S. Wilcove. 2008. “Is Oil Palm Agriculture Really Destroying Tropical
723 Biodiversity?” *Conservation Letters* 1 (2): 60–64. doi:10.1111/j.1755-263X.2008.00011.x.

724 Li, Li, Jinwei Dong, Simon Njeudeng Tenku, and Xiangming Xiao. 2015. “Mapping Oil Palm Plantations
725 in Cameroon Using PALSAR 50-m Orthorectified Mosaic Images.” *Remote Sensing* 7 (2): 1206–
726 24. doi:10.3390/rs70201206.

727 Li, Wang, Zheng Niu, Hanyue Chen, Dong Li, Mingquan Wu, and Wei Zhao. 2016. “Remote Estimation
728 of Canopy Height and Aboveground Biomass of Maize Using High-Resolution Stereo Images
729 from a Low-Cost Unmanned Aerial Vehicle System.” *Ecological Indicators* 67: 637–48.
730 doi:10.1016/j.ecolind.2016.03.036.

731 Li, Weijia, Haohuan Fu, Le Yu, and Arthur Cracknell. 2016. “Deep Learning Based Oil Palm Tree
732 Detection and Counting for High-Resolution Remote Sensing Images.” *Remote Sensing* 9 (1): 22.
733 doi:10.3390/rs9010022.

734 Lisein, Jonathan, Marc Pierrot-Deseilligny, Stéphanie Bonnet, and Philippe Lejeune. 2013. “A
735 Photogrammetric Workflow for the Creation of a Forest Canopy Height Model from Small
736 Unmanned Aerial System Imagery.” *Forests* 4 (4): 922–44. doi:10.3390/f4040922.

737 Lowe, David G. 2004. “Distinctive Image Features from Scale-Invariant Keypoints.” *International
738 Journal of Computer Vision* 60 (2): 91–110. doi:10.1023/B:VISI.0000029664.99615.94.

739 Malek, Salim, Yakoub Bazi, Naif Alajlan, Haikel AlHichri, and Farid Melgani. 2014. “Efficient
740 Framework for Palm Tree Detection in UAV Images.” *IEEE Journal of Selected Topics in Applied
741 Earth Observations and Remote Sensing* 7 (12): 4692–4703. doi:10.1109/JSTARS.2014.2331425.

742 Manandhar, Abhishek, Ludwig Hoegner, and Uwe Stilla. 2016. “Palm Tree Detection Using Circular
743 Autocorrelation of Polar Shape Matrix.” *ISPRS Annals of the Photogrammetry, Remote Sensing
744 and Spatial Information Sciences* 3 (July): 465–72. doi:10.5194/isprs-annals-III-3-465-2016.

745 Morel, Alexandra C., Joshua B. Fisher, and Yadvinder Malhi. 2012. “Evaluating the Potential to
746 Monitor Aboveground Biomass in Forest and Oil Palm in Sabah, Malaysia, for 2000-2008 with
747 Landsat ETM+ and ALOS-PALSAR.” *International Journal of Remote Sensing* 33 (11): 3614–39.
748 doi:10.1080/01431161.2011.631949.

749 Morel, Alexandra C., Sassan S. Saatchi, Yadvinder Malhi, Nicholas J. Berry, Lindsay Banin, David
750 Burslem, Reuben Nilus, and Robert C. Ong. 2011. “Estimating Aboveground Biomass in Forest
751 and Oil Palm Plantation in Sabah, Malaysian Borneo Using ALOS PALSAR Data.” *Forest Ecology
752 and Management* 262 (9): 1786–98. doi:10.1016/j.foreco.2011.07.008.

753 Nomura, Keiko, and Edward Mitchard. 2018. “More Than Meets the Eye: Using Sentinel-2 to Map
754 Small Plantations in Complex Forest Landscapes.” *Remote Sensing* 10 (11): 1693.
755 doi:10.3390/rs10111693.

756 O’Connor, James, Mike J. Smith, and Mike R. James. 2017. “Cameras and Settings for Aerial Surveys in
757 the Geosciences: Optimising Image Data.” *Progress in Physical Geography* 41 (3): 325–44.
758 doi:10.1177/0309133317703092.

759 Panagiotidis, Dimitrios, Azadeh Abdollahnejad, Peter Surový, and Vasco Chiteculo. 2017.
760 “Determining Tree Height and Crown Diameter from High-Resolution UAV Imagery.”
761 *International Journal of Remote Sensing* 38 (8–10): 2392–2410.

762 doi:10.1080/01431161.2016.1264028.

763 Puliti, Stefano, Liviu Theodor Ene, Terje Gobakken, and Erik Næsset. 2017. “Use of Partial-Coverage
764 UAV Data in Sampling for Large Scale Forest Inventories.” *Remote Sensing of Environment* 194:
765 115–26. doi:10.1016/j.rse.2017.03.019.

766 Puliti, Stefano, Hans Olerka, Terje Gobakken, and Erik Næsset. 2015. “Inventory of Small Forest Areas
767 Using an Unmanned Aerial System.” *Remote Sensing* 7 (8): 9632–54. doi:10.3390/rs70809632.

768 Rokhmana, Catur Aries. 2015. “The Potential of UAV-Based Remote Sensing for Supporting Precision
769 Agriculture in Indonesia.” *Procedia Environmental Sciences* 24: 245–53.
770 doi:10.1016/j.proenv.2015.03.032.

771 Roussel, Jean-Romain, and David Auty. 2018. “LidR: Airborne LiDAR Data Manipulation and
772 Visualization for Forestry Applications.” https://cran.r-project.org/package=lidR.

773 Shafri, Helmi Zulhaidi Mohd, and Nasrulhapiza Hamdan. 2009. “Hyperspectral Imagery for Mapping
774 Disease Infection in Oil Palm Plantation Using Vegetation Indices and Red Edge Techniques.”
775 *American Journal of Applied Sciences* 6 (6): 1031–35. doi:10.3844/ajassp.2009.1031.1035.

776 Silva, Carlos A., Andrew T. Hudak, Lee A. Vierling, E. Louise Loudermilk, Joseph J. O’Brien, J. Kevin
777 Hiers, Steve B. Jack, et al. 2016. “Imputation of Individual Longleaf Pine (Pinus Palustris Mill.)
778 Tree Attributes from Field and LiDAR Data.” *Canadian Journal of Remote Sensing* 42 (5): 554–73.
779 doi:10.1080/07038992.2016.1196582.

780 Srestasathiern, Panu, and Preesan Rakwatin. 2014. “Oil Palm Tree Detection with High Resolution
781 Multi-Spectral Satellite Imagery.” *Remote Sensing* 6 (10): 9749–74. doi:10.3390/rs6109749.

782 Thenkabail, Prasad S., Nicholas Stucky, Bronson W. Griscom, Mark S. Ashton, Jan Diels, Bauke Van der
783 Meer, and Eden Enclona. 2004. “Biomass Estimations and Carbon Stock Calculations in the Oil
784 Palm Plantations of African Derived Savannas Using IKONOS Data.” *International Journal of*
785 *Remote Sensing* 25 (23): 5447–72. doi:10.1080/01431160412331291279.

786 Thiel, Christian, and Christiane Schmullius. 2017. “Comparison of UAV Photograph-Based and
787 Airborne Lidar-Based Point Clouds over Forest from a Forestry Application Perspective.”
788 *International Journal of Remote Sensing* 38 (8–10): 2411–26.
789 doi:10.1080/01431161.2016.1225181.

790 Tonkin, Toby N., and Nicholas G. Midgley. 2016. “Ground-Control Networks for Image Based Surface
791 Reconstruction: An Investigation of Optimum Survey Designs Using UAV Derived Imagery and
792 Structure-from-Motion Photogrammetry.” *Remote Sensing* 8 (9): 16–19.
793 doi:10.3390/rs8090786.

794 Turner, Darren, Arko Lucieer, and Luke Wallace. 2014. “Direct Georeferencing of Ultrahigh-
795 Resolution UAV Imagery.” *IEEE Transactions on Geoscience and Remote Sensing* 52 (5): 2738–
796 45. doi:10.1109/TGRS.2013.2265295.

797 Wallace, Luke, Arko Lucieer, Zbyněk Malenovský, Darren Turner, and Petr Vopěnka. 2016.
798 “Assessment of Forest Structure Using Two UAV Techniques: A Comparison of Airborne Laser
799 Scanning and Structure from Motion (SfM) Point Clouds.” *Forests* 7 (3): 1–16.
800 doi:10.3390/f7030062.

801 Westoby, Matthew J., James Brasington, Neil F. Glasser, Michael J. Hambrey, and John M. Reynolds.
802 2012. “‘Structure-from-Motion’ Photogrammetry: A Low-Cost, Effective Tool for Geoscience
803 Applications.” *Geomorphology* 179: 300–314. doi:10.1016/j.geomorph.2012.08.021.

804 Zarco-Tejada, Pablo J., Rafael Diaz-Varela, Vincenzo Angileri, and Philippe Loudjani. 2014. “Tree
805 Height Quantification Using Very High Resolution Imagery Acquired from an Unmanned Aerial
806 Vehicle (UAV) and Automatic 3D Photo-Reconstruction Methods.” *European Journal of*
807 *Agronomy* 55: 89–99. doi:10.1016/j.eja.2014.01.004.

808 Zhang, Keqi, Shu Ching Chen, Dean Whitman, Mei Ling Shyu, Jianhua Yan, and Chengcui Zhang. 2003.
809 “A Progressive Morphological Filter for Removing Nonground Measurements from Airborne
810 LIDAR Data.” *IEEE Transactions on Geoscience and Remote Sensing* 41 (4 PART I): 872–82.
811 doi:10.1109/TGRS.2003.810682.

812

List of Figures

List of Tables